Lipid cubic phase with an organic–inorganic hybrid structure formed by organoalkoxysilane lipid

Miki Kariya, Kenichiro Omoto, Kaoru Nomura, Kento Yonezawa, Hironari Kamikubo, Toshio Nishino, Tomomi Inoie, Gwénaël Rapenne, Kazuma Yasuhara

Formation of lipid cubic phase with an organic-inorganic hybrid structure by organoalkoxysilane lipid

Miki Kariya,[a] Kenichiro Omoto,[a,‡,§,*] Kaoru Nomura,[b] Kento Yonezawa,[a,d] Hironari Kamikubo,[a] Gwénaël Rapenne[a,c] and Kazuma Yasuhara[a,d*]

[a] *Division of Materials Science, Nara Institute of Science and Technology (NAIST), 8916-5 Takayama-cho, Ikoma, 630-0192, Japan. yasuhara@ms.naist.jp*

[b] *Bioorganic Research Institute, Suntory Foundation for Life Sciences, 8-1-1 Seikadai, Seika-cho, Soraku-gun, Kyoto, 619-0284, Japan*

[c] *CEMES, Université de Toulouse, CNRS, 29 Rue Marvig, F-31055 Toulouse Cedex 4, France*

[d] *Center for Digital Green-innovation, Nara Institute of Science and Technology (NAIST), 8916-5 Takayama-cho, Ikoma, 630-0192, Japan*

[‡] *These authors contribute equally.*

[§] *Current address: Division of Chemistry and Materials Science, Graduate School of Engineering, Nagasaki University, 1-14 Bunkyo-machi, Nagasaki, 852-8521, Japan. omoto@nagasaki-u.ac.jp*

ABSTRACT : LIPID CUBIC PHASE ENCOMPASSING A CROSS-LINKED SILOXANE STRUCTURE WAS FORMED BY THE SELF-ASSEMBLY OF A SYNTHETIC ORGANOALKOXYSILANE LIPID IN WATER. THE SPONTANEOUS SOL-GEL REACTION OF THE ALKOXYSILANE MOIETY ON THE LIPID HEAD GROUP PRODUCED AN ORGANIC-INORGANIC HYBRID MATERIAL WITH A DOUBLE GYROID *Ia3d* CUBIC STRUCTURE.

The lipid bilayer is a key structure in cell membranes that plays important roles in biological systems.[1] A variety of naturally occurring phospholipids had been employed to assemble the lipid bilayer in the early studies of artificial cell membranes.[2] Also, many attempts have been made to form bilayer structures using synthetic lipids that enable the fine-tuning of membrane properties and functions due to their flexibility in molecular design.[3] Most of the previous studies of artificial lipids focused on the formation of lamellar structures such as vesicles and planar membranes. Although non-lamellar assemblies of lipids including cubic and hexagonal phases are also known to play important roles in cellular functions,[4,5] a limited number of researches have been reported for the formation of non-lamellar structures using synthetic lipids.[6]

In this study, we investigated the formation of the lipid cubic phase encompassing a polymerized ceramic-like siloxane network, which is spontaneously produced by the sol-gel reaction of a synthetic organosilane

lipid 1 (Fig. 1).[7] A lipid cubic phase is a class of non-lamellar lipid assemblies with regularly arranged structures composed of curved lipid bilayers and interpenetrating water channels.[4] Lipid cubic phases can accommodate both hydrophilic and hydrophobic molecules in water channels and bilayers, respectively, enabling various applications, such as a medium for the crystallization of membrane proteins[8] and cargo for drug delivery systems.[9] Several attempts have been previously made to introduce an organic-inorganic hybrid structure to artificial lipid membranes in a lamellar phase.[10] Synthetic lipids with an alkoxysilyl head group spontaneously form lipid bilayers with a ceramic-like siloxane on the surface of the lipid bilayer through the sol-gel reaction consisting of hydrolysis and following polycondensation in an aqueous solution. In particular, cerasome, an organic-inorganic hybrid vesicle[10a–e,g] as well as a hybrid bicelle,[10f] a discoidal lipid assembly with a siloxane surface have been developed so far. Introducing the ceramic-like layer to the lipid membrane contributed to improving their mechanical[10b,e,f] and thermal[10a] stabilities and modulating membrane properties such as permeability[10g]. To the best of our knowledge, this is the first report on the development of a lipid cubic phase with an organic-inorganic hybrid structure directed by the self-assembly of a synthetic lipid.

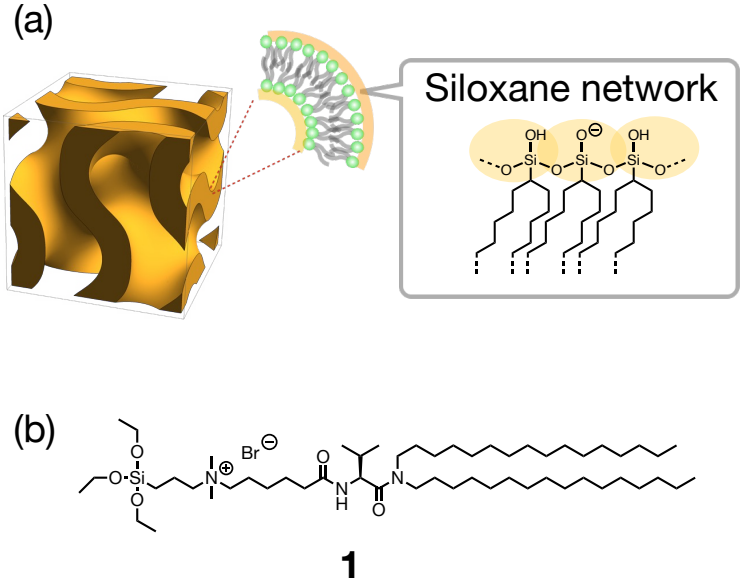

Fig. 1 (a) Schematic image of an organic-inorganic hybrid lipid cubic phase. (b) Chemical structure of the organosilane lipid (**1**) used in this study.

Organosilane lipid **1** was synthesized according to a literature procedure with a slight modification (see the supporting information and Scheme S1 for a detailed procedure).[10c] The sample was prepared by the hydration of the organosilane lipid **1** and introduced in a sealed capillary to avoid the unexpected evaporation of water as follows (Fig. S9).[11] First, **1** and water ([**1**] = 90 w/w%) were independently introduced into two different syringes which were connected by a coupler. The samples were mixed by repeatedly transferring the content between syringes for 500 cycles at 35 °C. The resulting transparent viscous mixture was loaded into the bottom of a glass capillary tube (1 mm diameter). The tube was sealed after centrifugation to remove air bubbles in the lipid-water mixture.

We first examined the hydrolysis and the cross-linking of lipid **1** which are the elementary processes of the sol-gel reaction. ^{1}H NMR measurement confirmed that the hydrolysis of the triethoxysilyl group was completed during high-temperature incubation at 60°C for 2 days, as the methylene signal at 3.83 ppm assigned to the triethoxysily group of **1** gradually disappeared concomitantly with the appearance of signals corresponding to ethanol at 3.73 ppm (Fig. S10). We evaluated the polymerization of lipid **1** by MALDI-TOF mass spectrometry. Mass spectrum of the lipid-water mixture taken after the high-temperature incubation for 2 days at 60 °C showed multiple peaks up to around m/z = 16000 at regular intervals (m/z = 890), corresponding to the polymerized lipid **1** smaller than 18mer (Fig. 2a). The solid-state ^{29}Si NMR spectrum of the sample showed three remarkable peaks at -50.0, -58.8, and -68.3 ppm, which correspond to primary (T1), secondary (T2) and tertiary (T3) siloxanes, respectively (Fig. 2b).[12] Considering the ratio of the integration for each signal, (T1: 5.7%, T2: 36.9%, T3: 57.4%) the polymerized lipid **1** with a branched structure seems to exist as a major species rather than a linear one.

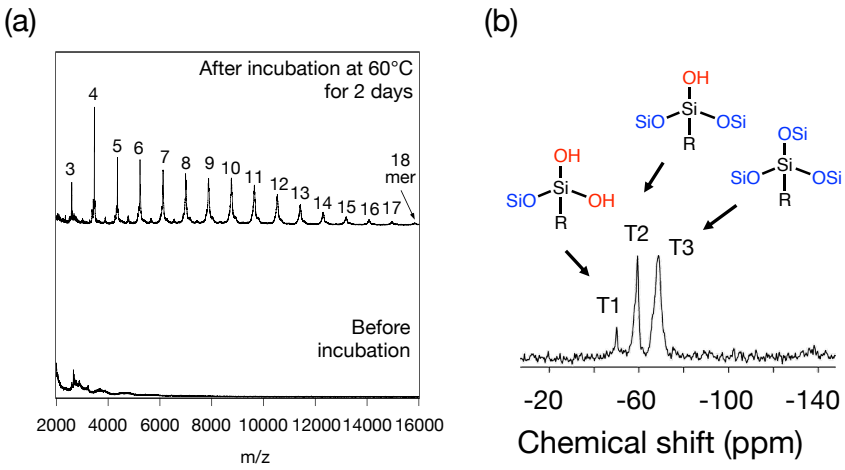

Fig. 2 (a) MALDI-TOF Mass spectrum (DCTB, positive) of the lipid-water mixtures ([**1**] = 90 w/w%). Spectrum of the sample before (bottom) and after (top) high-temperature incubation at 60°C for two days. (b) Solid-state ^{29}Si NMR spectrum of the lipid-water mixture ([**1**] = 90 w/w%) obtained after the high-temperature incubation.

Changes in the aggregation structure of the lipid-water mixture during the high-temperature incubation were qualitatively characterized using polarized optical microscopy (POM) which can differentiate the optical anisotropy of the sample (Fig. 3). For instance, optically anisotropic phases such as lamellar exhibit birefringence, while optically isotropic phases such as fluid isotropic and cubic phases do not.[13] The prepared lipid-water mixture showed only a dark field under a crossed-Nicole condition, reflecting the presence of an optically isotropic lipid assembly. After 7 hours of incubation of the sample at 60 °C, several domains showing birefringence appeared and gradually spread throughout the sample in 18 hours, suggesting the formation of an optically anisotropic phase such as a lamellar structure. With further incubation of the sample, the anisotropic domains with birefringence shrank and eventually disappeared in 2 days. We confirmed a similar process of transitions in several samples prepared independently, although the time required for the whole reaction somewhat varied (Fig. S11). Further incubation for up to 8 days showed no change in the optical anisotropy, suggesting the completion of the structural change of the lipid assembly within 2 days (Fig. S11).

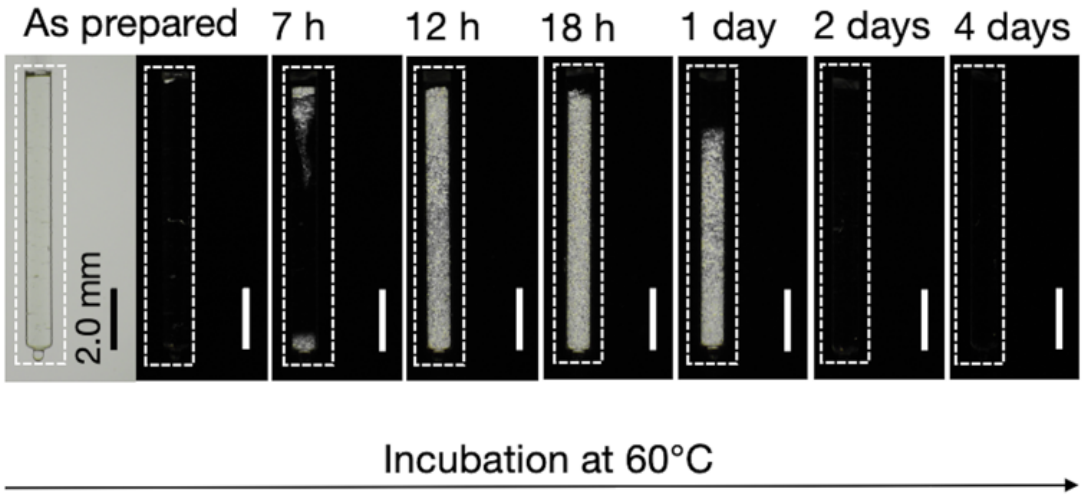

Fig. 3 Time course of the POM image traces of the lipid-water mixture ([**1**] = 90 w/w%) during high-temperature incubation in a sealed capillary. The leftmost panel corresponds to the bright field image of the as-prepared sample without polarizer and other dark images are crossed-Nicole images of the sample recorded at a certain incubation time as indicated. Scale bar: 2.0 mm.

Synchrotron small-angle X-ray scattering (SAXS) was performed to reveal the detailed nanostructure of the lipid-water mixture, which exhibits the significant incubation time dependence described above.[14] The optically isotropic sample obtained without high-temperature incubation showed a single broad peak around Q = 1.70 nm^{-1}, suggesting the random arrangement of lipid molecules without long-range order (black line in Fig. 4a). For the optically anisotropic sample obtained after an incubation of 13 hours, we observed only a sharp diffraction peak at 1.63 nm^{-1} (blue line in Fig. 4a), which can be assigned to a lamellar structure with an interlayer distance of d = 3.86 nm. Further incubation at 60 °C of the lipid-water mixture for 6 days, during which the sample became optically isotropic again, resulted in the appearance of multiple diffraction peaks in the SAXS spectrum (red line in Fig. 4a), suggesting the presence of a three-dimensional periodic nanostructure. The plots of the root sum of squares of assigned reflections ($(h^2 + k^2 + l^2)^{1/2}$) versus the observed Q-value confirmed the formation of the double gyroid cubic structure of the *Ia3d* space group with a lattice constant a = 9.7 nm (Fig. 4b). Since the spectrum did not change when X-ray was irradiated at different locations of the sample tube, we confirmed the homogeneity of the nanostructure in the entire tube. (Fig. S12). Notably, X-ray

diffractions with the same peak pattern were observed for the sample with a prolonged high-temperature incubation time of more than an additional 4 days that is consistent with the result of POM observation (Fig. S13).

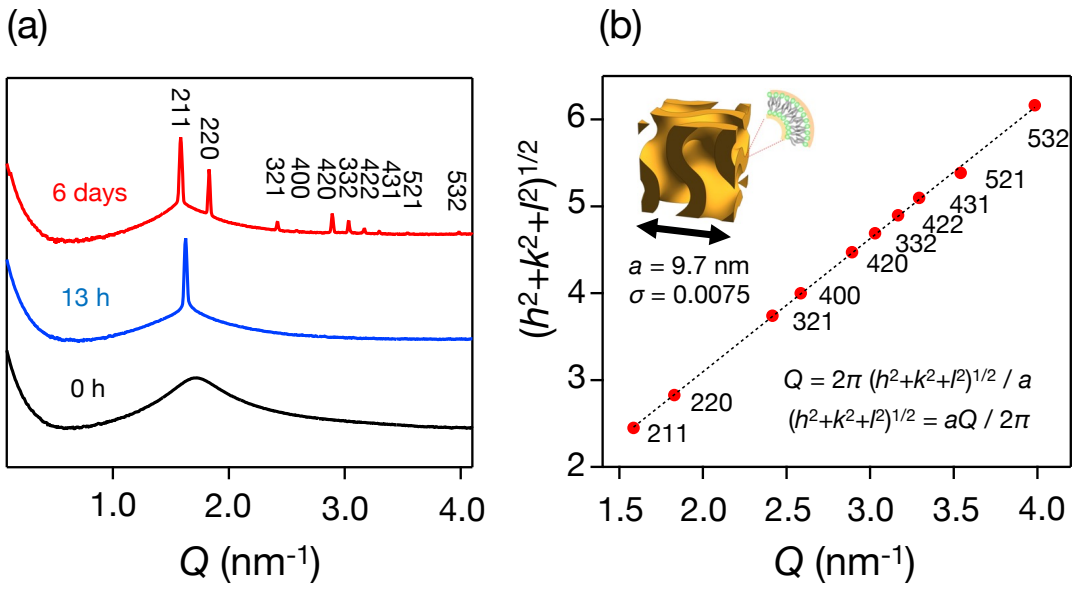

Fig. 4 (a) SAXS spectra of the lipid-water mixture ([**1**] = 90 w/w%) acquired after the high-temperature incubation for a certain time as indicated. The three-digit values on the peaks show the Miller indices. (b) Plots of the root sum of squares of assigned reflections ($(h^2 + k^2 + l^2)^{1/2}$) versus the measured Q-value for indexing *Ia3d* cubic peaks in the spectrum of the optically isotropic sample (6 days). All measurements are carried out at 60 °C.

According to the presented data, we propose a plausible mechanism by which lipid **1** forms the *Ia3d* cubic phase in a time-evolved manner. Lipid **1** forms a lamellar phase in the earlier stage when the intermolecular cross-linking is not completed, however, the completion of sol-gel reaction resulted in the formation of *Ia3d* cubic phase. The aggregation morphology of lipid molecules is generally governed by the geometry of the amphiphilic molecules, according to the concept of critical packing parameter.[17] In particular, the formation of cubic phases requires lipid molecules with a small hydrophilic head and relatively bulky hydrophobic groups that exhibit spontaneously negative membrane curvature. Although the detailed mechanism is beyond the scope of this paper, the data presented suggest the sol-gel reaction alters the amphiphilic geometry of lipid **1**. The hydrolysis of lipid **1**, by which the bulky ethoxysilyl group becomes a smaller silanol moiety as well as the subsequent polymerization contributes to

the reduction of the cross-sectional area of the hydrophilic headgroup, while the volume of the hydrophobic chains preserved. The resulting lipid assembly is likely to produce the negative spontaneous curvature that is favourable for the formation of the lipid cubic phase (Fig. S14).[4c]

In conclusion, we demonstrated the formation of an artificial lipid cubic phase with an organic-inorganic hybrid structure that is governed by the self-assembly and sol-gel reaction of a synthetic organosilane lipid. The polymerized siloxane layer was spontaneously formed by the high-temperature incubation of lipid-water mixture for several days. The completion of the sol-gel reaction resulted in the organic-inorganic hybrid material with a *Ia3d* cubic structure. Our finding in this study is expedited to provide a strategy to design new hybrid material with a non-bilayer structure using a synthetic lipid.

This work was financially supported in part by JSPS KAKENHI Grant-in-Aids for Scientific Research on Innovative Areas (Molecular Engine, No. 18H05419; G. R.), Young Scientists (No. 21K14478; K. O.), Transformative Research Areas A (Molecular Cybernetics, No. 21H05883; K. Y.), and Challenging Research (Exploratory, No. 21K19007; K.Y.), Kurita Water and Environment Foundation (20E057; K. O.) and Iketani Science and Technology Foundation (0321123-A; K.O.). The synchrotron radiation X-ray diffraction experiments were conducted on BL10C at the Photon Factory (Proposal No. 2020G579). We are grateful to Prof. Dr. Nobutaka Shimizu and Dr. Hideaki Takagi (Photon Factory, High Energy Accelerator Research Organization) for SAXS measurements. The authors thank Dr. Jun-ichi Kikuchi, Professor Emeritus, Nara Institute of Science and Technology, for fruitful discussions.

Notes and references

1 R. B. Gennis, *Biomembranes: Molecular Structure and Function*, Springer-Verlag, New York, 1989.

2 A. D. Bangham, *Prog. Biophys. Mol. Biol.*, 1968, **18**, 29–95.

3 (a) T. Kunitake and Y. Okahata, *J. Am. Chem. Soc.*, 1977, **99**, 3860–3861; (b) T. Kunitake, *Angew. Chem., Int. Ed. Engl.*, 1992, **31**, 709–726; (c) A. Mueller and D. F. O'Brien, *Chem. Rev.*, 2002, **102**, 727–758; (d) D. Y. Sasaki, T. A. Waggoner, J. A. Last and T. M. Alam, *Langmuir*, 2002, **18**, 3714–3721; (e) T. Hamada, R. Sugimoto, M. C. Vestergaard, T. Nagasaki and M. Takagi, *J. Am. Chem. Soc.*, 2010, **132**, 10528–10532; (f) A. M. Bayer, S. Alam, S. I. Mattern-Schain and M. D. Best, *Chem. Eur. J.*, 2014, **20**, 3350–3357; (g) A. G. Kohli, P. H. Kierstead, V. J. Venditto, C. L. Walsh and F. C. Szoka, *J. Controlled Release*, 2014, **190**, 274–287; (h) K. Sato, T. Muraoka and K. Kinbara, *Acc. Chem. Res.*, 2021, **54**, 3700–3709; (i) K. Yasuhara, K. Omoto, T. Nishino and G. Rapenne, in *Concepts and Design of Materials Nanoarchitectonics*, ed. O. Azzaroni and K. Ariga, Royal Society of Chemistry, Cambridge, 2022, ch. 16, pp. 361–380.

4 (a) M. L. Lynch and P. T. Spicer, *Bicontinuous Liquid Crystals*, CRC Press, Boca Ranton, 2005; (b) R. Koynova and B. Tenchov, *OA Biochem.*, 2013, **1**, 1–9; (c) R. Mezzenga, J. M. Seddon, C. J. Drummond, B. J. Boyd, G. E. Schröder-Turk and L. Sagalowicz, *Adv. Mater.*, 2019, **31**, 1900818.

5 (a) D. P. Siegel and R. M. Epand, *Biophys. J.*, 1997, **73**, 3089–3111; (b) S. Salentinig, S. Phan, A. Hawley and B. J. Boyd, *Angew. Chem. Int. Ed.*, 2015, **54**, 1600–1603; (c) A. J. Clulow, M. Salim, A. Hawley, B. J. Boyd, *Chem. Phys. Lipids*, 2018, **211**, 107–116; (d) N. W. Schmidt, A. Mishra, J. Wang, W. F. DeGrado and G. C. L. Wong, *J. Am. Chem. Soc.*, 2013, **135**, 13710–13719.

6 (a) Y.-S. Lee, J.-Z. Yang, T. M. Sisson, D. A. Frankel, J. T. Gleeson, E. Aksay, S. L. Keller, S. M. Gruner and D. F. O' Brien, *J. Am. Chem. Soc.*, 1995, **117**, 5573–5578; (b) R. Koynova, L. Wang and R. C. MacDonald, *Mol. Pharmaceutics*, 2008, **5**, 739–744; (c) R. Koynova, Boris Tenchov and R. C. MacDonald, *ACS Biomater. Sci. Eng*., 2015, **1**, 130–138; (d) L. S. Manni, S. Assenza, M. Duss, J. J. Vallooran, F. Juranyi, S. Jurt, O. Zerbe, E. M. Landau and R. Mezzenga, *Nat. Nanotechnol.*, 2019, **14**, 609–615.
7 K. Kuroda, A. Shimojima, K. Kawahara, R. Wakabayashi, Y. Tamura, Y. Asakura and M. Kitahara, *Chem. Mater.*, 2014, **26**, 211–220.
8 (a) E. M. Landau and J. Rosenbusch, *Proc. Natl. Acad. Sci. USA*, 1996, **93**, 14532–14535; (b) V. Cherezov, J. Clogston, M. Z. Papiz and M. Caffrey, *J. Mol. Biol.*, 2006, **357**, 1605–1618; (c) C. E. Conn and C. J. Drummond, *Soft Matter*, 2013, **9**, 3449–3464; (d) A. Zabara, J. T. Y. Chong, I. Martiel, L. Stark, B. A. Cromer, C. Speziale, C. J. Drummond and R. Mezzenga, *Nat Commun.*, 2018, **9**, 544.
9 J. Zhai, C. Fong, N. Tran and C. J. Drummond, *ACS Nano*, 2019, **13**, 6178–6206.
10 (a) K. Katagiri, K. Ariga and J. Kikuchi, *Chem. Lett.*, 1999, **28**, 661–662; (b) K. Katagiri, R. Hamasaki, K. Ariga and J. Kikuchi, *J. Am. Chem. Soc.*, 2002, **124**, 7892–7893; (c) K. Katagiri, M. Hashizume, K. Ariga, T. Terashima and J. Kikuchi, *Chem. Eur. J*., 2007, **13**, 5272–5281; (d) J. Kikuchi and K. Yasuhara, *Advances in Biomimetics*, ed. A. George, IntechOpen, Rijeka, 2011, 231–250; (e) T. Kawataki, K. Yasuhara and J. Kikuchi, *Chem. Lett.*, 2011, **40**, 461–463; (f) K. Yasuhara, S. Miki, H. Nakazono, A. Ohta and J. Kikuchi, *Chem. Commun*., 2011, **47**, 4691–4693; (g) K. Yasuhara, T. Kawataki, S. Okuda, S. Oshima and J. Kikuchi, *Chem. Commun*., 2013, **49**, 665–667.
11 M. Caffrey and V. Cherezov, *Nat. Protoc.*, 2009, **4**, 706–731.
12 (a) S. Sakamoto, A. Shimojima, K. Miyasaka, J. Ruan, O. Terasaki and K. Kuroda, *J. Am. Chem. Soc.*, 2009, **131**, 9634–9635; (b) K. Fujii, S. Hayashi, H. Hashizume, S. Shimomura, K. Jimura, T. Fujita, N. Iyi, A. Yamagishi, H. Sato and T. Ando, *Phys. Chem. Chem. Phys.*, 2016, **18**, 19146–19157.
13 P. G. Hartley and H.-H Shen, in *Self-Assembled Supramolecular Architectures: Lyotropic Crystals*, ed. N. Garti, P. Somasundaran and R. Mezzenga, John Wiely & Sons. Inc., Hoboken, 2012, ch. 4, pp. 97–127.
14 A. I. Tyler, R. V. Law and J. M. Seddon, in *Method in Membrane Lipids*, ed. D. M. Owen, Springer, New York, 2nd edn, 2015, ch. 16, pp. 199–225.
15 R. Bärenwald, A. Achilles, F. Lange, T. M. Ferreira and K. Saalwächter, *Polymers*, 2016, **8**, 439.
16 S. Matuoka, S. Kato, M. Akiyama, Y. Amemiya and I. Hatta, *Biochim. Biophys. Acta*, *Biomembr.*, 1990, **1028**, 103–109.
17 J. N. Israelachivili, *Intermolecular and Surface Forces*, Elsevier Academic Press, Amsterdam, 3rd edn, 2017.

Supporting Informations

1. Abbreviation

DCM: dichloromethane, DCTB: *trans*-2-[3-(4-*tert*-butylphenyl)-2-methyl-2-propenylidene]malononitrile, DIEA: *N*,*N*-diisopropylethylamine, DMF: *N*,*N*-dimethylformamide, HBTU: hexafluorophosphate benzotriazole tetramethyl uronium, HRMS: high resolution mass spectrometry, MALDI-TOF MS: matrix-assisted laser desorption ionization time-of-flight mass spectrometry, MeCN: acetonitrile, MeOH: methanol, NMR: nuclear magnetic resonance, PEG: polyethylene glycol, POM: polarized optical microscope, SAXS: small angle X-ray scattering, TEA: triethylamine, TEM: transmission electron microscopy, THF: tetrahydrofuran, TMS: tetramethylsilane.

2. Synthesis of organosilane lipid 1

Materials and methods

Organosilane lipid **1** was synthesized according to a literature procedure with a slight modification.[1] All solvents, organic and inorganic reagents are commercially available and were used without further purification unless otherwise stated. Solution state NMR spectroscopy was performed using a JEOL JNM-ECA600 and a JEOL JNM-ECX400P spectrometers. TMS ($Si(CH_3)_4$) = 0 ppm) and $CDCl_3$ ($CDCl_3$ = 77.16 ppm) were used as an internal reference for ^1H and ^{13}C NMR measurements in $CDCl_3$ respectively. HRMS was performed using a JEOL spiral TOF (JMS-S3000) using DCTB as a matrix and PEG as an internal standard. GPC was performed using a JAI JC-908W-C60BW with two polystyrene gel columns connected in series (JAIGEL 1H and 2H) with a mobile phase of $CHCl_3$.

Scheme S1. Synthetic route for **1**.

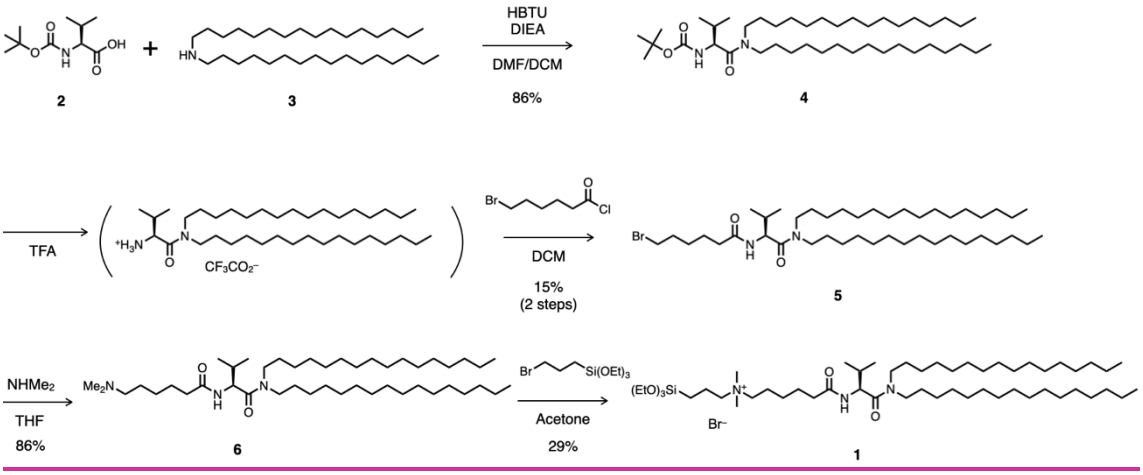
HBTU
DIEA
DMF/DCM
86%
2
3
4
TFA
DCM
15%
(2 steps)
5
NHMe2
THF
86%
6
Acetone
29%
1

Preparation of *N*,*N*-dihexadecyl-*N*$^{\alpha}$-(*tert*-butoxycarbonyl)-L-valineamide (4)

N-(*tert*-butoxycarbonyl)-L-valine (**2**) (2.34 g, 10.8 mmol, 1.0 eq), *N,N*-dihexadecylamine (**3**) (4.00 g, 10.7 mmol, 1.0 eq), and HBTU (5.12 g, 13.5 mmol, 1.3 eq) were placed in a two-necked flask. The inner gas was replaced by N_2 and anhydrous DMF (16 mL), anhydrous DCM (20 mL), and DIEA (4.5 mL) were added. After stirring at room temperature for 20 h, the reaction mixture was concentrated by evaporation of solvents at reduced pressure. After adding EtOAc (200 mL), the reaction mixture was washed successively with H_2O (150 mL) and saturated aqueous solution of $NaHCO_3$ (150 mL x 4) followed by brine (100 mL x 3). The organic layer was dried over Na_2SO_4, filtered, and evaporated under reduced pressure to obtain a crude product as a pale brown oil. The crude product was purified by column chromatography (SiO_2, *n*-hexane/EtOAc = 6/1) to afford **4** (6.13 g, 9.22 mmol, 86%) as a colourless oil.

^{1}H NMR (600 MHz, $CDCl_3$, 293 K, Fig. S1): δ (ppm) = 5.26 (d, 1H, J = 9.1 Hz, CON*H*CH), 4.39 (dd, 1H, J = 9.2, 6.7 Hz, NHC*H*CO), 3.63–3.56 (m, 1H, NC*H*H$(CH_2)_{14}CH_3$), 3.40–3.33 (m, 1H, NC*H*H$(CH_2)_{14}CH_3$), 3.24–3.17 (m, 1H, NC*H*H$(CH_2)_{14}CH_3$), 3.04–2.98 (m, 1H, NC*H*H$(CH_2)_{14}CH_3$), 1.91 (m, 1H, $(CH_3)_2$C*H*CH), 1.64–1.42 (m, 4H, N$(CH_2$C*H*$_2(CH_2)_{13}CH_3)_2$), 1.42 (s, 9H, $(CH_3)_3$CO), 1.31–1.22 (m, 52H, N$(CH_2CH_2(CH_2)_{13}CH_3)_2$), 0.94 (d, 3H, J = 6.9 Hz, C*H*$_3$CHC*H*$_3$), 0.90 (d, 3H, J = 6.9 Hz, C*H*$_3$CHC*H*$_3$), 0.88 (t, 6H, J = 7.0 Hz, N$((CH_2)_{15}CH_3)_2$).

^{13}C NMR (150 MHz, $CDCl_3$, 293 K, Fig. S2): δ (ppm) = 171.90, 155.81, 100.06, 79.34, 55.10, 48.07, 46.05, 32.30, 32.08, 29.85, 29.81, 29.73, 29.70, 29.56, 29.54, 29.52, 29.41, 28.47, 27.75, 27.17, 26.99, 22.84, 19.78, 17.53, 14.28.

HRMS (MALDI): calcd. for $[C_{42}H_{84}O_3 + Na]^+$: m/z = 687.6371, found: m/z = 687.6375.

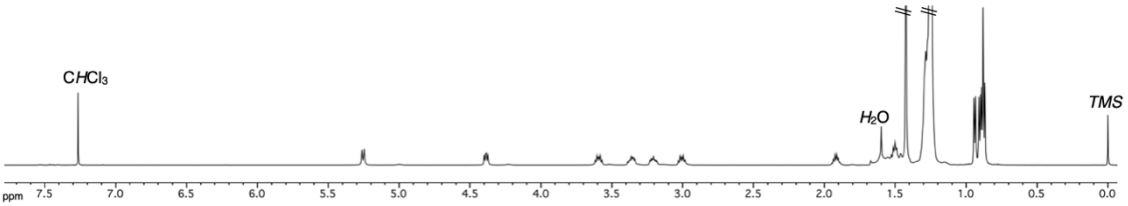

Fig. S1 ^{1}H NMR spectrum of **4** (600 MHz, $CDCl_3$, 293 K).

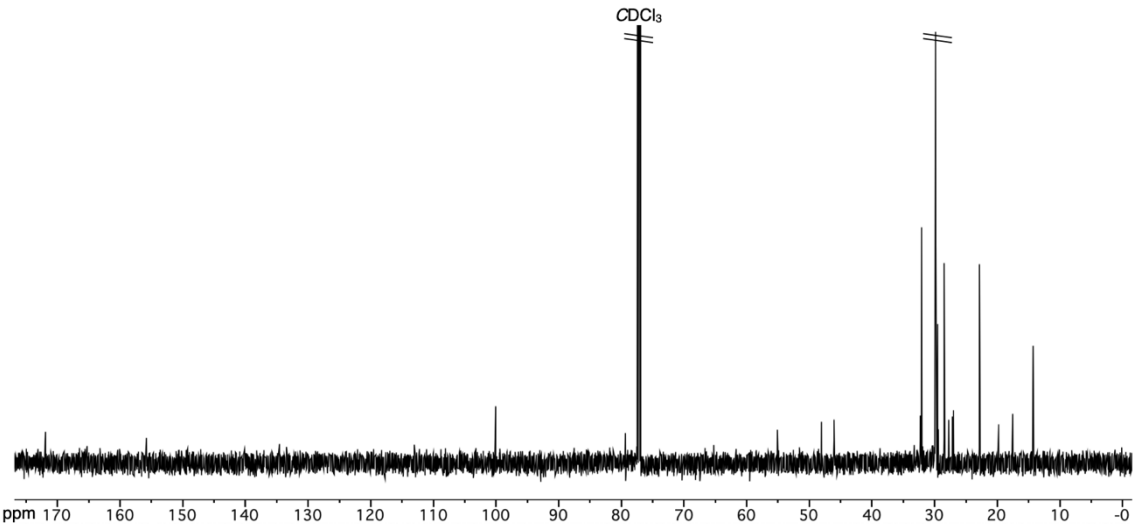

Fig. S2 ^{13}C NMR spectrum of **4** (150 MHz, $CDCl_3$, 293 K).

Preparation of *N*,*N*-dihexadecyl-N^{α}-(6-bromohexanoyl)-L-valineamide (5)

4 (6.05 g, 9.11 mmol, 1.0 eq) was placed in a flask. After adding TFA (8.5 mL), the mixture was stirred at room temperature for 15.5 h. After adding DCM (20 mL), the solvent was evaporated under reduced pressure to obtain a colourless oil. The inner gas of the flask was replaced by N_2 and anhydrous DCM (40 mL) and TEA (10.5 mL) were added. After cooling down to 0 °C, 6-bromohexanoyl chloride (10 mL, 9.8 g, 74.3 mmol, 8.2 eq) was added dropwise over 15 min. After stirring at room temperature for 20 h, H_2O (20 mL) and DCM (100 mL) were added to the mixture. The organic phase was washed with a saturated aqueous solution of $NaHCO_3$ (100 mL x 4) followed by brine (100 mL x 3). The organic layers were combined and dried over Na_2SO_4, filtered, and the solvent was evaporated under reduced pressure to obtain a crude product as a brown oil. The crude product was purified by column chromatography (SiO_2, *n*-hexane/DCM = 1/0–0/1) followed by reprecipitation from cold MeOH to afford **5** (2.42 g, 1.35 mmol, 15%) as a colourless solid.

^{1}H NMR (600 MHz, $CDCl_3$, 293 K, Fig. S3): δ (ppm) = 6.18 (d, 1H, J = 8.8 Hz, CON*H*CH), 4.77 (dd, 1H, J = 8.6, 6.6 Hz, NHC*H*CO), 3.60–3.53 (m, 1H, NC*H*H$(CH_2)_{14}CH_3$), 3.40 (t, 2H, J = 6.8 Hz, BrC*H*$_2(CH_2)_4$CO), 3.38–3.33 (m, 1H, NC*H*H$(CH_2)_{14}CH_3$), 3.26–3.20 (m, 1H, NC*H*H$(CH_2)_{14}CH_3$), 3.05–3.99 (m, 1H, NC*H*H$(CH_2)_{14}CH_3$), 2.22 (t, 2H, J = 7.5 Hz, Br$(CH_2)_4$-C*H*$_2$CO), 1.97 (m, 1H, $(CH_3)_2$C*H*CH), 1.87 (tt, J = 7.2, 7.2 Hz, 2H, BrCH$_2$C*H*$_2(CH_2)_3$CO), 1.71–1.62 (m, 2H, N$(CH_2)_3$C*H*$_2$CH$_2$CO), 1.61–1.54 (m, 6H, NCH$_2$C*H*$_2(CH_2)_3$CO, N(CH$_2$C*H*$_2(CH_2)_{13}CH_3)_2$), 1.36–1.22 (m, 54H, N(CH$_2$CH$_2$(C*H*$_2)_{13}CH_3)_2$, N$(CH_2)_2$C*H*$_2$CH$_2$CO),

0.95 (d, 3H, J = 6.5 Hz, CH_3CHCH_3), 0.90 (d, 3H, J = 6.5 Hz, CH_3CHCH_3), 0.88 (t, 6H, J = 7.1 Hz, N((CH_2)$_{15}$CH_3)$_2$).

^{13}C NMR (150 MHz, $CDCl_3$, 293 K, Fig. S4): δ (ppm) = 172.31, 171.54, 53.42, 48.08, 46.14, 36.65, 33.69, 32.61, 32.28, 32.08, 29.85, 29.81, 29.73, 29.52, 29.47, 29.37, 27.92, 27.74, 26.16, 26.98, 24.95, 22.85, 19.89, 17.71, 14.28.

HRMS (MALDI) mass: calcd. for [$C_{43}H_{85}N_2BrO_2$ + Na]$^+$: m/z = 763.5687, found: m/z = 763.5620.

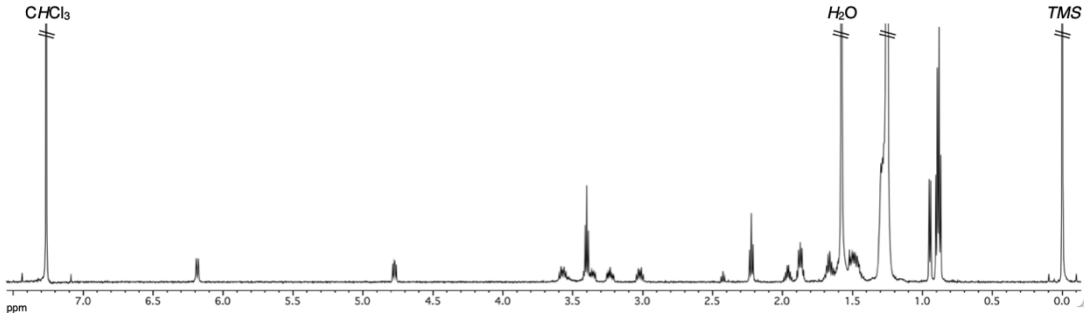

Fig. S3 ^{1}H NMR spectrum of **5** (600 MHz, $CDCl_3$, 293 K).

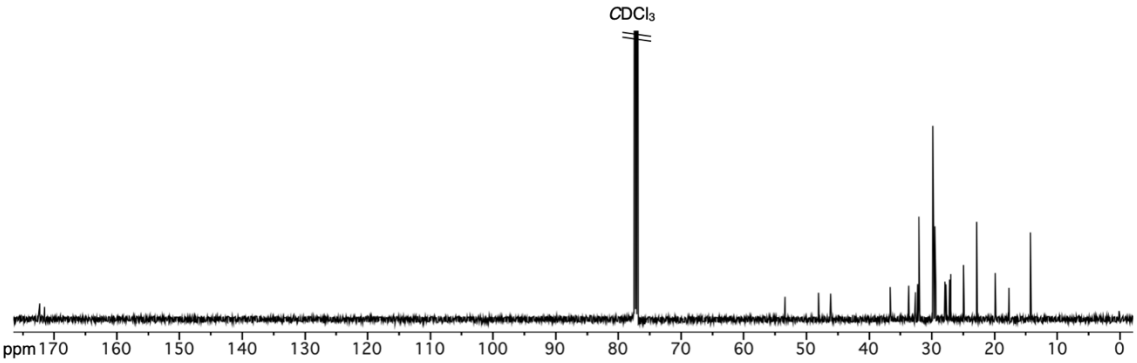

Fig. S4 ^{13}C NMR spectrum of **5** (150 MHz, $CDCl_3$, 293 K).

Preparation of *N*,*N*-dihexadecyl-*N*$^{\alpha}$-[6-(dimethylamino)hexanoyl]-L-valineamide (6)

A THF solution of $NHMe_2$ (ca. 2 M, 20 mL, ca. 40 mmol, ca. 15 eq) was added in a flask containing **5** (2.01 g, 2.71 mmol, 1.0 eq). The mixture was stirred at room temperature for 17.5 h. The reaction mixture was evaporated under N_2 flow to obtain a crude product as a colourless solid. The crude product was purified by reprecipitation in MeCN to afford **6** (1.65 g, 2.34 mmol, 86%) as a colourless solid.

^{1}H NMR (600 MHz, $CDCl_3$, 293 K, Fig. S5): δ (ppm) = 6.17 (d, 1H, J = 8.9 Hz, CON*H*CH), 4.77 (dd, 1H, J = 9.0, 6.4 Hz, NHC*H*CO), 3.60–3.51 (m, 1H, NC*H*H$(CH_2)_{14}CH_3$), 3.40–3.32 (m, 1H, NC*H*H$(CH_2)_{14}CH_3$), 3.28–3.21 (m, 1H, NC*H*H$(CH_2)_{14}CH_3$), 3.06–2.99 (m, 1H, NC*H*H$(CH_2)_{14}CH_3$), 2.25–2.19 (m, 4H, NC$H_2(CH_2)_3$CH_2CO), 2.19 (s, 6H, $(CH_3)_2$N$(CH_2)_5$CO), 1.96 (m, 1H, $(CH_3)_2$C*H*CH), 1.69–1.62 (m, 2H, N$(CH_2)_3$CH_2CH_2CO), 1.61–1.44 (m, 6H, NCH_2C$H_2(CH_2)_3$CO, N$(CH_2$C$H_2(CH_2)_{13}CH_3)_2$), 1.36–1.22 (m, 54H, N$(CH_2)_2(CH_2)_{13}CH_3)_2$, N$(CH_2)_2CH_2(CH_2)_2$CO), 0.94 (d, 3H, J = 6.5 Hz, CH_3CHCH_3), 0.90 (d, 3H, J = 6.5 Hz, CH_3CHCH_3), 0.88 (t, 6H, J = 6.8 Hz, N$((CH_2)_{15}CH_3)_2$).

^{13}C NMR (150 MHz, $CDCl_3$, 293 K, Fig. S6): δ (ppm) = 172.62, 171.58, 59.77, 53.38, 48.07, 46.13, 45.62, 36.92, 32.26, 32.06, 29.84, 29.80, 29.72, 29.51, 29.46, 29.37, 27.73, 27.59, 27.26, 27.16, 26.98, 25.83, 22.83, 19.87, 17.73, 14.27.

HRMS (MALDI): calcd. for $[C_{45}H_{91}N_3O_2 + H]^+$: m/z = 706.7184, found: m/z = 706.7164.

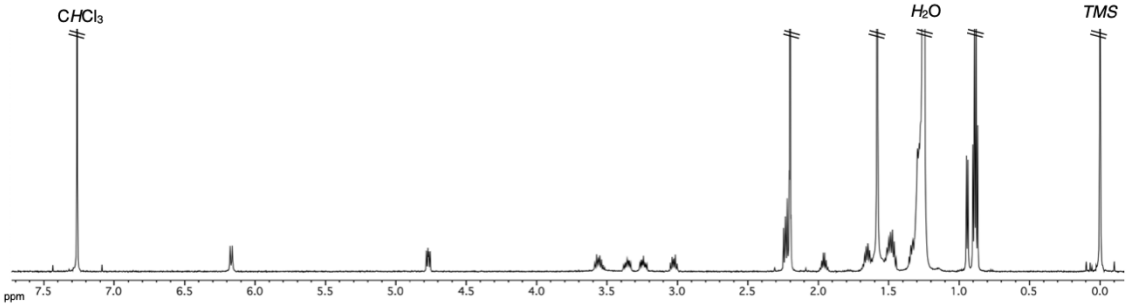

Fig. S5 ^{1}H NMR spectrum of **6** (600 MHz, $CDCl_3$, 293 K).

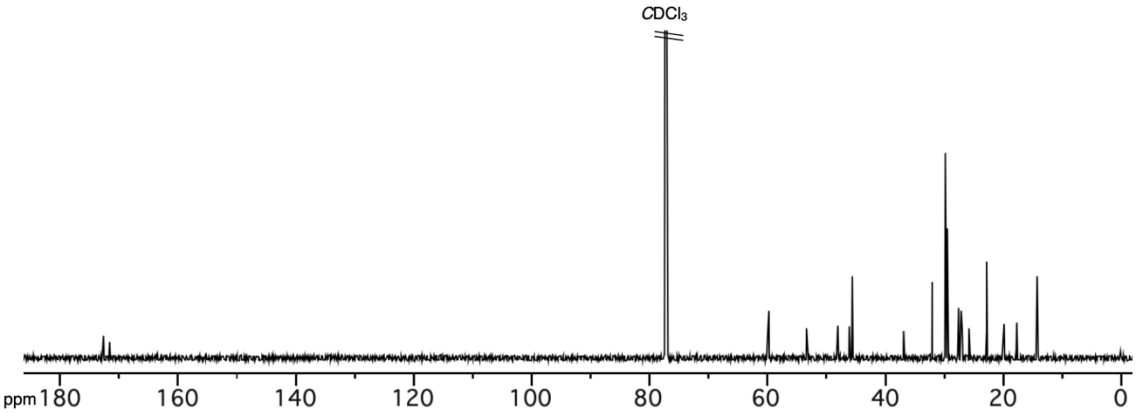

Fig. S6 ^{13}C NMR spectrum of **6** (150 MHz, $CDCl_3$, 293 K).

Preparation of *N*,*N*-dihexadecyl-*N*$^{\alpha}$-[6-[(3-triethoxysilyl)propyldimethylammonio]-hexanoyl]-L-valineamide bromide (1)

In a flask containing a solution of **6** (2.74 g, 3.89 mmol, 1.0 eq) in anhydrous acetone (8.0 mL) under N_2 was added (3-bromopropyl)triethoxysilane (5.1 mL, 6.63 g, 27.3 mmol, 7.0 eq). After stirring the mixture at room temperature for 6 days, the solvent was removed by evaporation under reduced pressure to obtain a crude product as a colourless oil. The crude product was purified by GPC ($CHCl_3$) to afford **1** (1.13 g, 1.16 μmol, 29%) as a colourless oil.

^{1}H NMR (600 MHz, $CDCl_3$, 293 K, Fig. S7): δ (ppm) = 6.42 (d, 1H, J = 8.5 Hz, CON*H*CH), 4.71 (dd, 1H, J = 8.4, 6.8 Hz, NHC*H*CO), 3.83 (q, 6H, J = 7.1 Hz, $(CH_3CH_2O)_3Si$), 3.61–3.46 (m, 5H, NC*H*H$(CH_2)_{14}CH_3$, $CH_2CH_2N^+CH_2CH_2$), 3.34 (s, 3H, $CH_2N^+(CH_3)(CH_3)CH_2$), 3.33 (s, 3H, $CH_2N^+(CH_3)(CH_3)CH_2$), 3.33 (m, 1H, NC*H*H$(CH_2)_{14}CH_3$), 3.25 (m, 1H, NC*H*H$(CH_2)_{14}CH_3$), 3.00 (m, 1H, NC*H*H$(CH_2)_{14}CH_3$), 2.35 (dt, 1H, J = 7.2 and 14.4 Hz, $N^+(CH_2)_4CHHCO$), 2.24 (dt, 1H, J = 7.2 and 14.4 Hz, $N^+(CH_2)_4CHHCO$), 1.98 (m, 1H, $(CH_3)_2CHCH$), 1.86–1.76 (m, 2H, $N^+CH_2CH_2(CH_2)_3CO$), 1.76–1.69 (tt, 2H, J = 7.4 and 7.4 Hz, $N^+CH_2CH_2(CH_2)_3CO$), 1.66–1.52 (m, 2H, $N^+(CH_3)_2CH_2CH_2CO$), 1.52–1.47 (m, 2H, $NCH_2CH_2(CH_2)_{13}CH_3$), 1.47–1.40 (m, 2H, $NCH_2CH_2(CH_2)_{13}CH_3$), 1.32–1.20 (m, 54H, $N(CH_2CH_2(CH_2)_{13}CH_3)_2$, $N^+(CH_2)_2CH_2CH_2$), 1.23 (t, 9H, J = 7.2 Hz, $(CH_3CH_2O)_3Si$), 0.95 (d, 3H, J = 6.8 Hz, CH_3CHCH_3), 0.91 (d, 3H, J = 6.8 Hz, CH_3CHCH_3), 0.88 (t, 6H, J = 7.0 Hz, $N((CH_2)_{15}CH_3)_2$), 0.67 (t, 2H, J = 7.8 Hz, $SiCH_2$).

^{13}C NMR (150 MHz, $CDCl_3$, 293 K, Fig. S8): δ (ppm) = 172.17, 171.43, 65.73, 64.00, 58.81, 53.73, 51.36, 48.10, 46.20, 35.78, 32.03, 31.90, 29.81, 29.71, 29.68, 29.51, 29.47, 29.42, 29.33, 27.73, 27.17, 27.02, 25.70, 24.92, 22.80, 22.49, 19.90, 18.45, 17.82, 16.79, 14.24, 6.95.

HR-MS (MALDI): calcd. for $[C_{54}H_{112}N_3O_5Si]^+$: m/z = 910.8368, found: m/z = 910.8388.

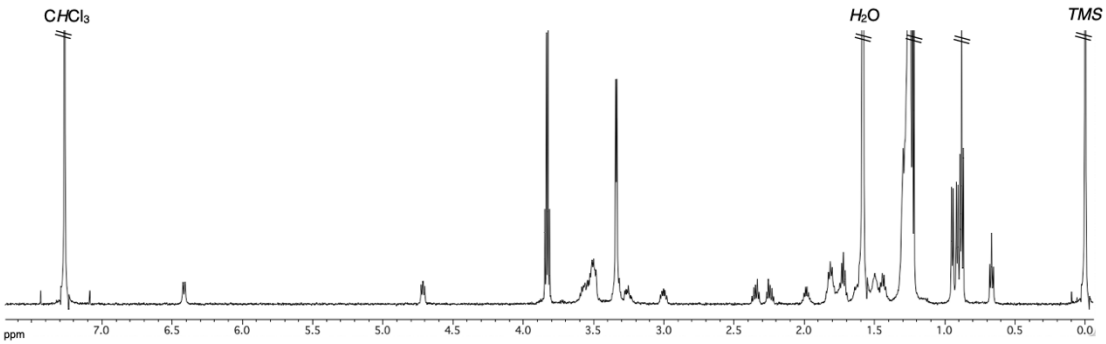

Fig. S7 ^{1}H NMR spectrum of **1** (600 MHz, $CDCl_3$, 293 K).

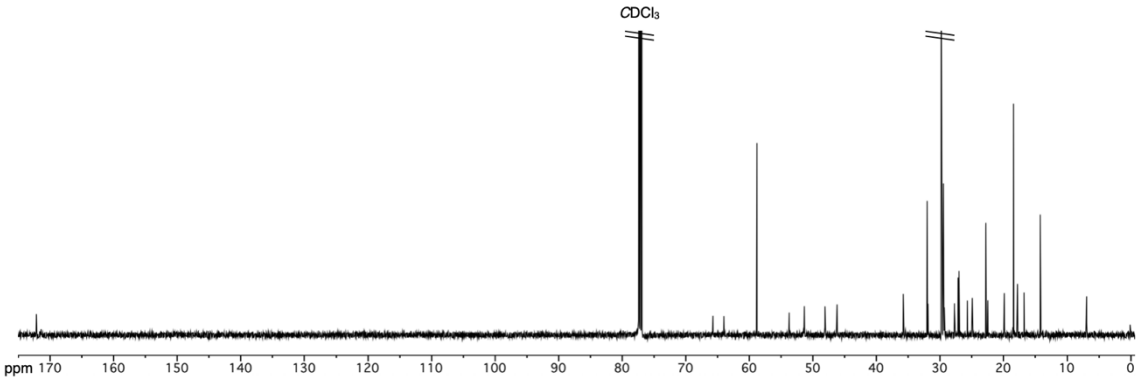

Fig. S8 ^{13}C NMR spectrum of **1** (150 MHz, $CDCl_3$, 293 K).

3. Preparation and characterization of organic-inorganic hybrid lipid cubic phase

Experimental procedures

Typical procedure for the preparation of lipid-water mixture ([**1**] = 90 w/w%)

1 (26.89 mg) and water (2.99 mg) were independently introduced into two different syringes which were connected by a coupler (Fig. S9a). The samples were mixed by repeatedly transferring the content between syringes for 500 cycles at 35 °C. The resulting transparent viscous lipid-water mixture was loaded into the bottom of the glass capillary tube (1 mm diameter). After centrifugation to remove air bubbles in the mixture, the open end of the capillary was sealed by flame fusing of the glass with a burner and protected by coating with melted wax to avoid the unexpected evaporation of water (Fig. S9b).

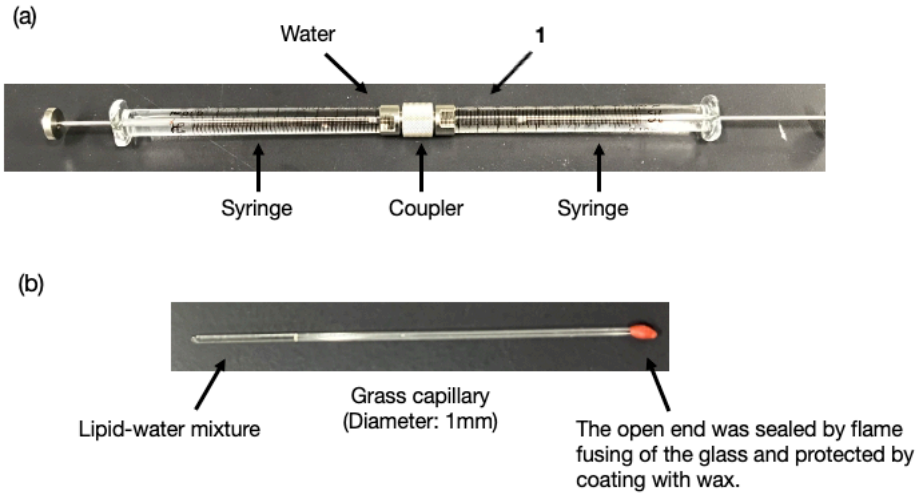

Fig. S9 (a) Two syringes each containing water and **1** which were connected by a coupler. (b) A sealed capillary containing a lipid-water mixture ([**1**] = 90 w/w%).

Solution state ^{1}H NMR spectroscopy of the lipid-water mixture

Lipid-water mixtures ([**1**] = 90 w/w%) in different sealed capillaries were subjected to the high-temperature incubation at 60 °C for a certain time. The resulted samples were removed from the capillaries and dissolved in $CDCl_3$. ^{1}H NMR spectra of the resulted solutions were measured (Fig. S10).

MALDI-TOF MS of the lipid-water mixture

Lipid-water mixture ([**1**] = 90 w/w%) in a sealed capillary was subjected to the high-temperature incubation at 60 °C for 2 days. The resulted sample was removed from the capillary and dissolved in $CHCl_3$. MALDI-TOF MS of the resulted solution was performed with a Bruker Autoflex II using DCTB as a matrix (Fig. S11).

POM observation of the lipid-water mixture

Lipid-water mixtures ([**1**] = 90 w/w%) in different sealed capillaries were subjected to the high-temperature incubation at 60 °C using a heating stage (TOKAI HIT TPi-SZX2X) equipped with an Olympus binocular stereomicroscope (SZX2-ILLTQ). The time courses of the POM image traces of the samples during high-temperature incubation were recorded (Fig. S12).

Solid-state NMR spectroscopy of the lipid-water mixture

Lipid-water mixture ([**1**] = 90 w/w%) in a sealed syringe was subjected to high-temperature incubation at 60 °C for 7 days. The resulting sample was removed from the syringe and sealed in a zirconium cell. Solid-states ^{29}Si NMR spectrum (60 °C, Fig. 2b in the main text) was measured using a Bruker Avance III 600 (Bruker Biospin, AG, Switzerland) equipped with a narrow-bore magnet operated at a ^{1}H resonance frequency of 600 MHz. Data were recorded using an VTN double-resonance 4 mm magic angle spinning (MAS) probe, at spinning speeds of 5 kHz. The ^{29}Si spectra were collected with a 4 μs excitation pulses and a 250 s recycle delay. The ^{29}Si NMR spectrum was also measured with sample tube alone and subtracted to exclude background signals. The ^{29}Si chemical shifts were externally referenced to hexamethylcyclotrisiloxane (-9.5 ppm).[2]

SAXS measurement of the lipid-water mixture

Lipid-water mixtures ([**1**] = 90 w/w%) in sealed capillaries were subjected to high-

temperature incubation at 60 °C for a certain time. SAXS of the resulting samples were measured at a controlled temperature using a synchrotron X-ray beam (λ = 1.00 Å) of BL-10C at the Photon Factory, Japan, equipped with a customized temperature controller (INSTEC HCS302-LN190) and a Dectoris model PIRATUS 2M detector (Fig. 4 and 5 in the main text and Fig. S13).

Experimental Data

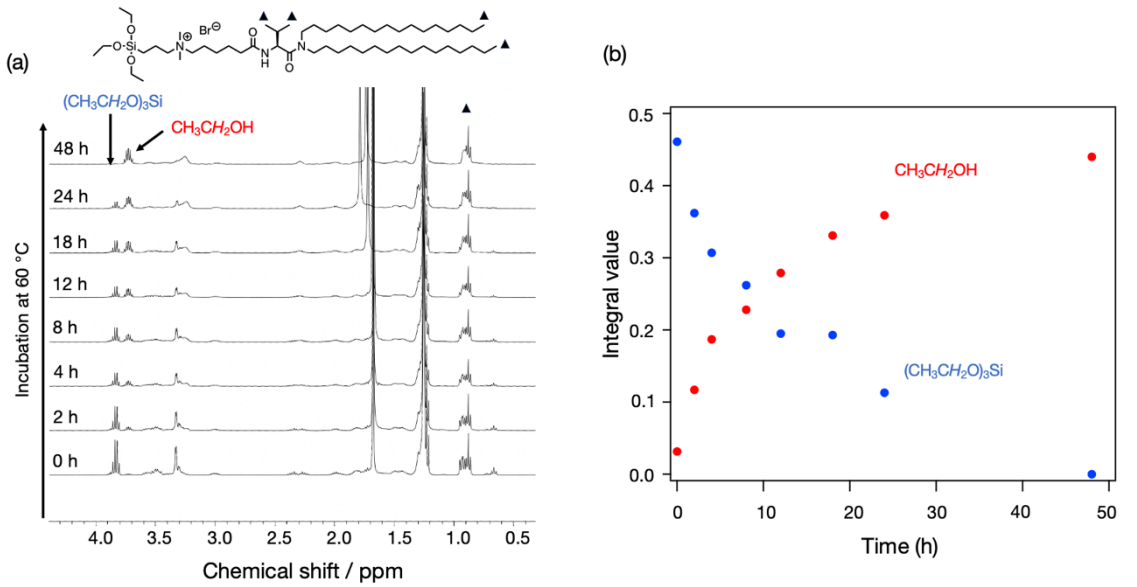

Fig. S10 (a) ^{1}H NMR (400 MHz, $CDCl_3$, 293 K) spectra of the lipid-water mixture ([**1**] = 90 w/w%) acquired after the high-temperature incubation for a certain time as indicated. (b) Time course change in the integral values of methylene (CH_2) signals at 3.83 ppm and 3.73 assigned as triethoxysilyl group ($(CH_3CH_2)_3Si$) and ethanol (CH_3CH_2OH). The integral values were evaluated by taking the sum of the integral values of peaks at 0.95–0.85 ppm as 1.00 as a standard which are assigned as the CH_3 groups of the hexadecyl chains and isopropyl group of **1** and its derivatives (labelled with filled triangles in Fig. S10).

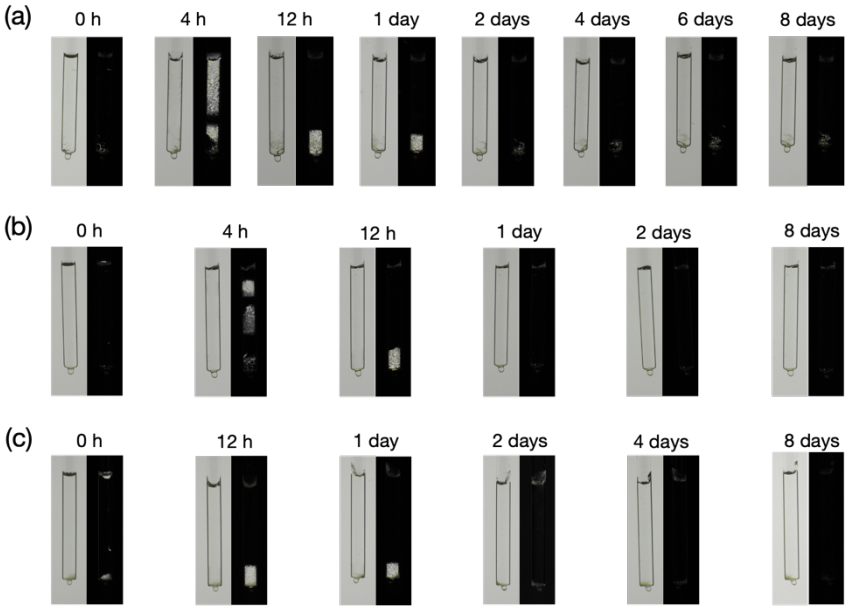

Fig. S11 Time courses of the POM image traces of the lipid-water mixtures ([**1**] = 90 w/w%) in sealed capillaries during high-temperature incubation (recorded at 60 °C). The left images are bright field images of the samples without polarizer and the dark images on the right are crossed-Nicole images of the samples recorded at a certain incubation time as indicated. Three different samples (a–c) were observed independently.

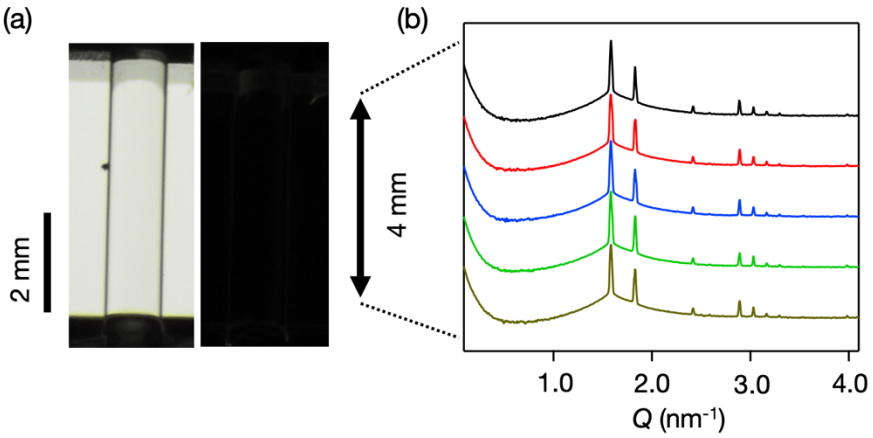

Fig. S12 (a) POM image of the lipid-water mixture ([**1**] = 90 w/w%) in a sealed capillary after high-temperature incubation for 6 days (recorded at 60 °C). The left is a bright field image of the sample without a polarizer and the right is a crossed-Nicole image of the sample. (b) SAXS spectra of the lipid-water mixture ([**1**] = 90 w/w%) in a sealed capillary acquired after the high-temperature incubation for 6 days (recorded at 60 °C). X-ray was irradiated at different locations on the sample shown in the panel (a).

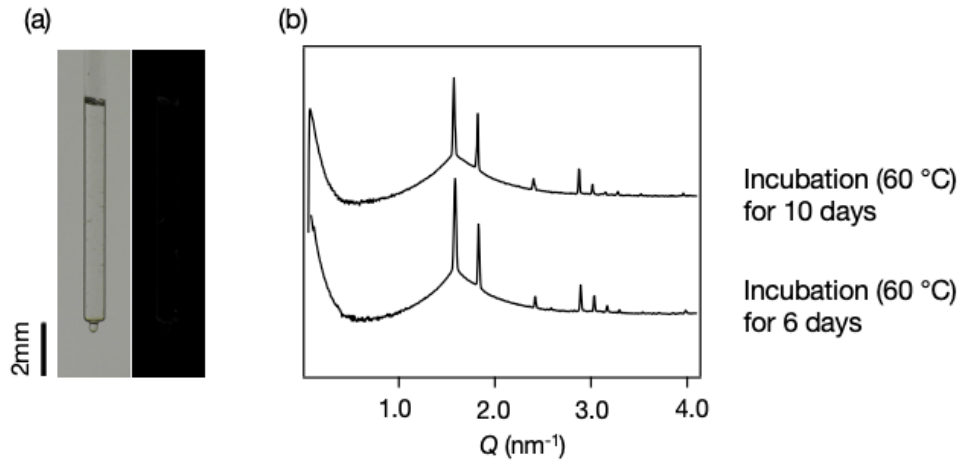

Fig. S13 (a) POM image of the lipid-water mixture ([**1**] = 90 w/w%) in a sealed capillary after high-temperature incubation for 10 days (recorded at 60 °C). The left is a bright field image of the sample without a polarizer and the right is a crossed-Nicole image of the sample. (b) SAXS spectra of the lipid-water mixture ([**1**] = 90 w/w%) in a sealed capillary acquired after the high-temperature incubation for 10 days (top) and 6 days (bottom) (recorded at 60 °C).

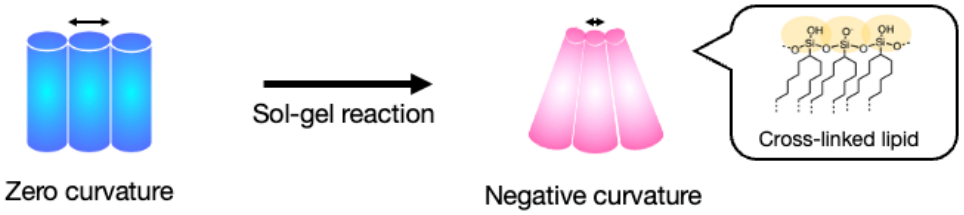

Fig. S14 Schematic image explaining the plausible mechanism of lipid cubic phase formation by sol-gel reaction. Hydrolysis and cross-linking of the lipid headgroup decreases the apparent cross-sectional area of the lipid head group whereas the volume of the hydrophobic chain was maintained, resulting in the negative spontaneous curvature of lipid assembly.

4. Reference

1. K. Katagiri, M. Hashizume, K. Ariga, T. Terashima and J. Kikuchi, *Chem. Eur. J.*, 2007, **13**, 5272–5281.
2. H. Marsmann, 29Si-NMR spectroscopic results, *in Oxygen-17 and Silicon-29 NMR spectroscopy*, Springer Verlag, Berlin, Heidelber, New York 1981.